AIP | Applied Physics Letters

A face-shear mode single crystal ultrasonic motor

Shiyang Li, Wenhua Jiang, Limei Zheng, and Wenwu Cao

Citation: Applied Physics Letters **102**, 183512 (2013); doi: 10.1063/1.4804627
View online: http://dx.doi.org/10.1063/1.4804627
View Table of Contents: http://scitation.aip.org/content/aip/journal/apl/102/18?ver=pdfcov
Published by the AIP Publishing

A face-shear mode single crystal ultrasonic motor

Shiyang Li,[1,2,a)] Wenhua Jiang,[2] Limei Zheng,[2,3] and Wenwu Cao[2,3,b)]
[1]*Department of Instrument Science and Engineering, Shanghai Jiao Tong University, Shanghai 200240, China*
[2]*Materials Research Institute, The Pennsylvania State University, University Park, Pennsylvania 16802, USA*
[3]*Condensed Matter Science and Technology Institute, Harbin Institute of Technology, Harbin 150080, China*

(Received 2 April 2013; accepted 27 April 2013; published online 10 May 2013)

We report a face-shear mode ultrasonic motor (USM) made of $[011]_c$ poled Zt ± 45° cut $0.24Pb(In_{1/2}Nb_{1/2})O_3$-$0.46Pb(Mg_{1/3}Nb_{2/3})O_3$-$0.30PbTiO_3$ single crystal, which takes advantage of the extremely large $d_{36} = 2368$ pC/N. This motor has a maximum no-load linear velocity of 182.5 mm/s and a maximum output force of 1.03 N under the drive of $V_p = 50$ V, f = 72 kHz. Compared with the k_{31} mode USM made of $Pb(Zr,Ti)O_3$ (PZT), our USM has simpler structure, lower driving frequency, much higher electromechanical coupling factor, and twice power density. This USM can be used for low frequency operation as well as cryogenic actuation with a large torque. © *2013 AIP Publishing LLC*. [http://dx.doi.org/10.1063/1.4804627]

Piezoelectric ultrasonic motors (USMs) have been used in high-precision mechanical systems due to their unique characteristics, such as high power density, low speed with high torque, no electromagnetic noise, and compact size. Various types of USM have been reported in the past three decades.[1–11] With the discovery of new generation piezoelectric materials, i.e., the relaxor-PT ferroelectric single crystals, such as $(1-x)Pb(Mg_{1/3}Nb_{2/3})O_3$-$xPbTiO_3$ (PMN-PT) and $(1-x)Pb(Zn_{1/3}Nb_{2/3})O_3$-$xPbTiO_3$ (PZN-PT), high performance USMs have been developed utilizing their superior piezoelectric and electromechanical coupling properties.[12] In addition, these single crystals have very good actuation performance at low temperatures. Piezoelectric ultrasonic motors made of PMN-PT single crystals have been fabricated and tested at cryogenic temperatures.[13,14] However, the low coercive field (2.5 kV/cm) of binary PMN-PT crystal limits its applications. Since the ternary $(1-x-y)Pb(In_{1/2}Nb_{1/2})O_3$-$yPb(Mg_{1/3}Nb_{2/3})O_3$-$xPbTiO_3$ (PIN-PMN-PT) single crystals retain similar electro-mechanical coupling factors and piezoelectric coefficients as that of binary PMN–PT single crystals, but have significantly larger coercive field (>5 kV/cm),[12,15] they are much better for USM applications. Recently, a double-mode ultrasonic actuator made of ternary PIN-PMN-PT single crystal has been reported, which shows much improved performance.[16] All previously reported ultrasonic motors only used k_{31} or k_{33} mode in $[001]_c$ pseudo-cubic direction poled single Relaxor-PT single crystals.

Recently, the face-shear mode single crystal poled along $[011]_c$ with Zt ± 45° cut has drawn a lot of attention due to its ultralow frequency constant, high elastic compliances ($S_{66}^E > 120\,pm^2/N$), and much higher piezoelectric coefficients d_{36} (1600–2800 pC/N), which equals to the combined values of the two transverse piezoelectric coefficients $d_{36} = d'_{31} - d'_{32}$($d'_{31}, d'_{32}$ are piezoelectric coefficients before rotation).[17] Moreover, the face-shear mode crystals have significantly higher mechanical quality factor Q_m (150 to 180) than that of thickness-shear crystal based on k_{15} mode (20 to 30). Unlike the k_{15} type of shear mode resonator, the face-shear mode crystals will not be de-poled in operation because the poling electrodes are the same as the operating electrodes.[17–20] Owing to these unique properties, face-shear mode single crystals have immense potential for high power and low frequency devices.

In this letter, we report a single crystal USM operated in the face-shear mode. Fig. 1 shows the configuration and orientation of the single crystal ultrasonic actuator, which is made of $[011]_c$-polarized rhombohedral phase $0.24Pb(In_{1/2}Nb_{1/2})O_3$-$0.46Pb(Mg_{1/3}Nb_{2/3})O_3$-$0.30PbTiO_3$ (0.24PIN-0.46PMN-0.30PT) single crystal. It was grown by the modified Bridgman method and has the macroscopic symmetry of *mm2* after poling, and the crystal was oriented by the Laue X-ray diffraction machine with an accuracy of ±0.5°.

The orientations of the plate are $[0\bar{1}1]_c$, $[100]_c$, and $[011]_c$ along the length, width, and thickness directions with the dimensions of 9.6 mm (L) × 9.6 mm (W) × 2.5 mm (T) after polishing, respectively. Those pseudo-cubic directions correspond to the X, Y, and Z directions of the orthorhombic coordinates. A face-shear mode plate was prepared by rotating 45° angle about the $[011]_c$ (Z-direction), designated as *Zt* 45° cut. This square plate was sputtered with gold electrodes on the pair of $[011]_c$ surface (the two large planes) and fully poled along its thickness direction with a field of 10 kV/cm in silicone oil at room temperature. There is a gap of 0.5 mm between the two excitation electrodes on the upper surface as shown in Fig. 1. The bottom surface is fully coated to serve as the ground. Copper wires were bonded to electrode surfaces using silver epoxy for electrical connection.

Fig. 2(a) illustrates the structure of our face-shear mode single crystal USM. The motor consists of 0.24PIN-0.46PMN-0.30PT single crystal actuator, rotor, nylon plate with V-groove, and preload mechanics. The friction element is glued at the driving tip of the square single crystal plate, which is in contact with the rotor. The actuator is excited by a sinusoidal voltage signal to one of the electrodes on the upper surface. The other electrode on the upper surface is left floating. By adjusting the preload mechanics, a preload force can be applied between the actuator and the rotor.

To analyze the working principle, the finite element software, ANSYS (ANSYS, Inc., Canonsburg, PA) was used to

a)Electronic mail: shiyangli@sjtu.edu.cn
b)Electronic mail: dzk@psu.edu

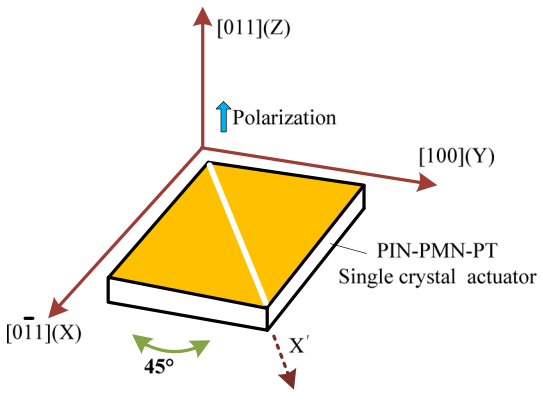

FIG. 1. Schematic of Zt 45° cut PIN-PMN-PT single crystal actuator.

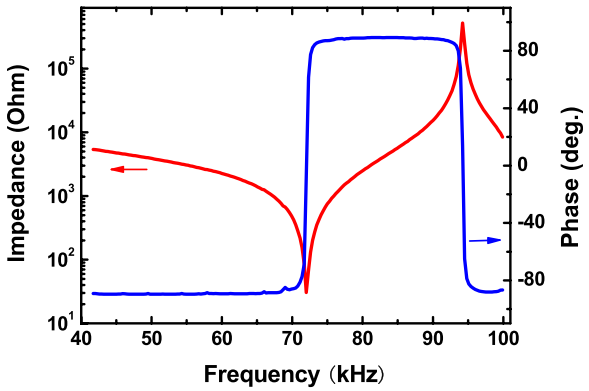

FIG. 3. The measured electrical impedance and phase spectra of the single crystal actuator.

simulate the vibration of this actuator. The material constants of 0.24PIN-0.46PMN-0.30PT single crystal reported in Ref. 15 were used in our simulations. The piezoelectric coefficient d_{36} is 2368 pC/N after *Zt* 45° rotation. In the harmonic analysis, the resonance response of the actuator is simulated under the action of a sine voltage signal with the voltage amplitude $V_p = 30$ V applied on one of electrodes on the upper surface. The damping is set to be 0.003. A face-shear vibration mode can be found at the resonant frequency 69.9 kHz by the harmonic analysis. The vibration shape of face-shear mode of PIN-PMN-PT single crystal actuator under the asymmetric excitation is shown in Fig. 2(b). The vertical displacement and horizontal displacement of the driving tip at the face-shear resonant frequency were extracted. The motion trajectory of the driving tip can be obtained from FEM simulation and is shown in Fig. 2(c). It can be seen that both vertical and horizontal motions are generated simultaneously at the driving tip under an electric field excitation. For a sinusoidal ac electric field, the driving tip oscillates

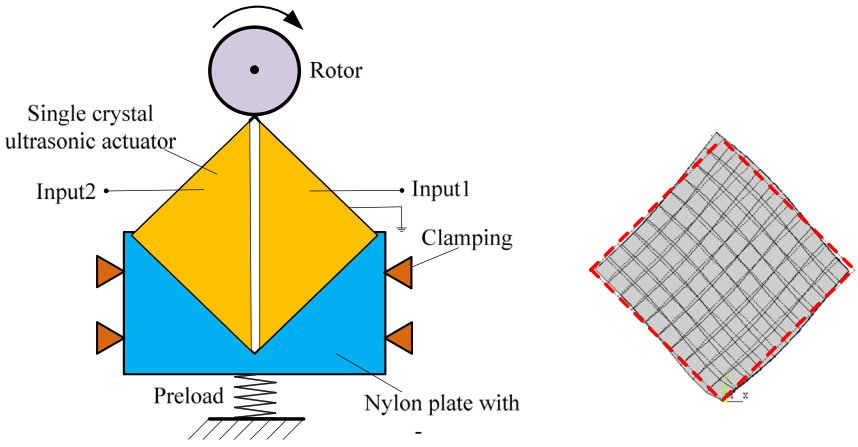

(a)

(b)

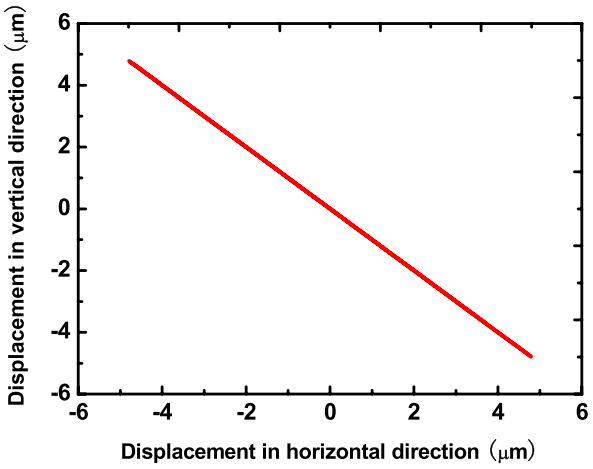

(c)

FIG. 2. Face-shear PIN-PMN-PT single crystal ultrasonic motor: (a) motor configuration, (b) mode shape of the stator, and (c) motion trajectory of the driving tip.

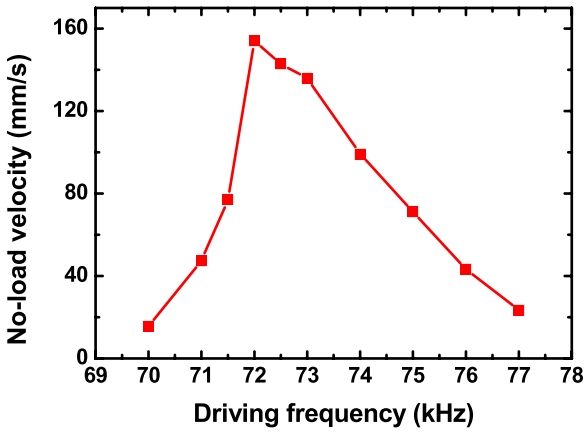

FIG. 4. Frequency versus no-load linear velocity under the drive of an ac field with $V_p = 30$ V.

along an inclined line with respect to the vertical direction. Whenever the driving tip is in contact with the rotor, a tangential friction force will produce a torque propelling the rotor to rotate as illustrated in Fig. 2(a).

The electrical impedance and phase spectrum of the single crystal actuator was measured at room temperature by an HP 4194A impedance-gain-phase analyze with a 16048A test fixture (Fig. 3). The measured face-shear resonant frequency f_s is 71.5 kHz, agrees with the calculated value within the experimental error.

Next, we assemble the prototype of single crystal motor as illustrated in Fig. 2(a). The preload force is kept constant in the experiment. A function generator and power amplifier were used to generate the driving signal. Fig. 4 shows the relationship between the frequency and no-load linear velocity at the driving tip derived by measuring the cycle number of the rotor in unit time when the voltage amplitude V_p is 30 V. We found a maximum linear velocity of 154 mm/s under the drive of $V_p = 30$ V, $f = 72$ kHz. When the frequency is away the resonant frequency, the velocity will decrease gradually. The relationship between the driving voltage and no-load linear velocity at the driving tip at 72 kHz is shown in Fig. 5. The motor can work well at a very low driving voltage of $V_p = 10$ V. The velocity increases monotonically with the amplitude of the driving voltage and gradually saturates when V_p is above 50 V.

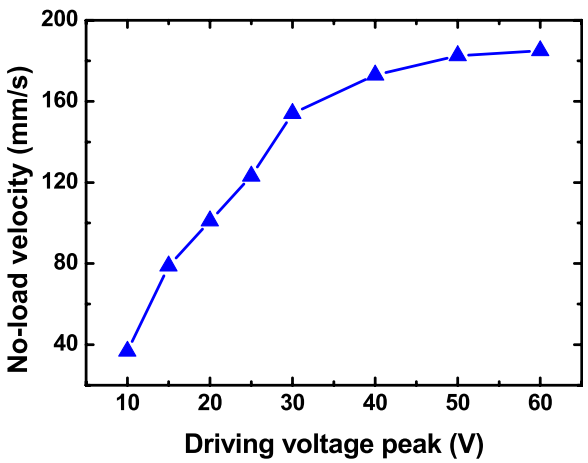

FIG. 5. Driving voltage versus no-load linear velocity at $f = 72$ kHz.

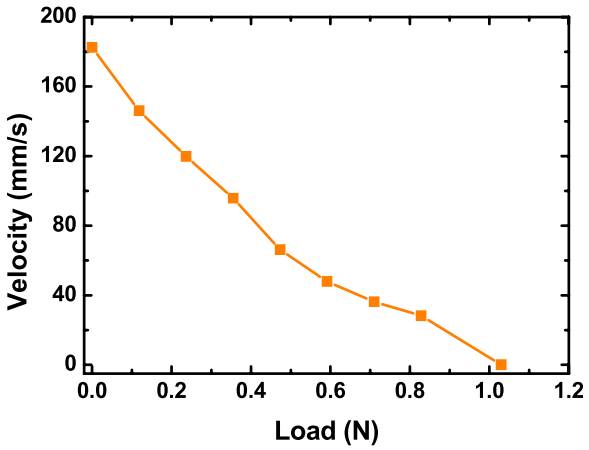

FIG. 6. Load versus linear velocity under the drive of an ac field with $V_p = 50$ V, $f = 72$ kHz.

The load torque is measured using the hanging weight method. Under the driving voltage of $V_p = 50$ V and $f = 72$ kHz, the relationship between the load and linear velocity at the driving tip is shown in Fig. 6. The maximum no-load linear velocity is 182.5 mm/s and the maximum output force reaches 1.03 N under the electrical drive of $V_p = 50$ V and $f = 72$ kHz.

To further evaluate the USM performance, our motor is compared with a k_{31} mode piezoelectric ultrasonic motor with square-plate actuator[21] in Table I. We use the effective electromechanical coupling factor k_{eff} to evaluate the energy conversion performance of the motor,[10,22] which can be calculated from the series and parallel resonance frequencies, and values for the two types of USM are shown in Table I. One can see that k_{eff} of face-shear mode single crystal USM is 0.65 while the k_{eff} of k_{31} mode PZT USM is only about 0.30. Such a high electromechanical coupling factor k_{eff} of the face-shear motor is due to the very high d_{36} (2368 pC/N) and k_{36} (~0.88 calculated by $k_{36} = d_{36}/\sqrt{\varepsilon_{33}^T s_{66}^E}$) of the piezoelectric single crystal. On the other hand, k_{31} for PZT piezoelectric ceramics is only ~0.33. Table I also shows that our motor only needs one phase of the driving voltage, and it has lower resonant frequency although our motor has smaller volume than the k_{31} mode USM with a square-plate actuator. The power density of our motor is 1.48×10^{-4} W/mm^3, which is more than two times of the power density of k_{31} mode PZT USM.

TABLE I. Performance comparison between k_{36} mode USM and k_{31} mode USM with square-plate shape.

	k_{36} mode USM[a]	k_{31} mode USM[b]
Material	PIN-PMN-PT	PZT
Volume V (mm^3)	$9.6 \times 9.6 \times 2.5$	$15 \times 15 \times 2$
f_r (kHz)	72	92
Driving phase number	One	Two
Stall Force (N)	1.03 N ($V_p = 50$ V)	1 N ($V_p = 50$ V)
Power density (W/mm^3)	1.48×10^{-4}	7.11×10^{-5}
Electromechanical coupling factor k_{eff}	0.65	0.30

[a]Our work.
[b]Ref. 21.

In summary, a face-shear mode single-crystal ultrasonic motor has been developed and characterized. This motor takes advantage of the extremely large piezoelectric coefficient $d_{36} = d_{31}$-d_{32} (2368 pC/N) in $[011]_c$ poled Zt ± 45° cut 0.24PIN-0.46PMN-0.30PT single crystal. We designed the USM using finite element simulation and confirmed the superiority of the design experimentally. Compared with the k_{31} mode PZT USM with square-plate actuator, our face-shear mode USM has simpler structure, lower driving frequency, twice the electromechanical coupling factor and more than double the power density, which means higher efficiency, less energy loss, and suppressed temperature rise during operation. This face-shear mode single crystal USM can be used for low frequency operations as well as cryogenic actuators with a very large torque.

This research was supported in part by the National Key Basic Research Program (973) of China under Grant No. 2013CB632900 and one of the authors (Shiyang Li) acknowledges the National Natural Science Foundation of China (Grant No. 81027001) and China Scholarship Council for the oversea study program.

[1]S. Cagatay, B. Koc, and K. Uchino, IEEE Trans. Ultrason. Ferroelectr. Freq. Control **50**, 782 (2003).
[2]B. Koc, S. Cagatay, and K. Uchino, IEEE Trans. Ultrason. Ferroelectr. Freq. Control **49**, 495 (2002).
[3]C. S. Zhao, *Ultrasonic Motors: Technologies and Applications* (Science Press, Beijing, 2011).
[4]J. Rho, K. Oh, H. Kim, and H. Jung, IEEE Trans. Ultrason. Ferroelectr. Freq. Control **54**, 715 (2007).
[5]J. Friend, L. Yeo, and M. Hogg, Appl. Phys. Lett. **92**, 014107 (2008).
[6]F. Giraud and B. Semail, IEEE Trans. Ultrason. Ferroelectr. Freq. Control **53**, 1468 (2006).
[7]A. Frangi a, A. Corigliano, M. Binci, and P. Faure, Ultrasonics **43**, 747 (2005).
[8]C. Y. Lu, X. Tian, T. Y. Zhou, and Y. Chen, Ultrasonics **44**, e585 (2006).
[9]Y. X. Liu, W. S. Chen, J. K. Liu, and S. J. Shi, IEEE Trans. Ultrason. Ferroelectr. Freq. Control **57**, 2360 (2010).
[10]Y. X. Liu, J. K. Liu, W. S. Chen, and S. J. Shi, IEEE Trans. Ultrason. Ferroelectr. Freq. Control **59**, 981 (2012).
[11]Y. Ming, Z. Meiling, R. C. Richardson, M. C. Levesley, P. G. Walker, and K. Watterson, Sens. Actuators, A **119**, 214 (2005).
[12]S. J. Zhang and F. Li, J. Appl. Phys. **111**, 031301 (2012).
[13]S. X. Dong, L. Yan, N. Wang, D. Viehland, X. Jiang, P. Rehrig, and W. Hackenberger, Appl. Phys. Lett. **86**, 53501 (2005).
[14]S. X. Dong, L. Yan, D. Viehland, X. Jiang, and W. Hackenberger, Appl. Phys. Lett. **92**, 153504 (2008).
[15]E. Sun, W. Cao, and P. Han, Mater. Lett. **65**, 2855 (2011).
[16]M. S. Guo, S. X. Dong, B. Ren, and H. S. Luo, IEEE Trans. Ultrason. Ferroelectr. Freq. Control **57**, 2596 (2010).
[17]S. J. Zhang, W. H. Jiang, R. J. Meyer, F. Li, J. Luo, and Wenwu Cao, J. Appl. Phys. **110**, 064106 (2011).
[18]S. J. Zhang, F. Li, W. H. Jiang, J. Luo, R. J. Meyer, Wenwu Cao, and T. R. Shrout, Appl. Phys. Lett. **98**, 182903 (2011).
[19]K. Kim, S. J. Zhang, and X. N. Jiang, Appl. Phys. Lett. **100**, 253501 (2012).
[20]K. Kim, S. J. Zhang, and X. N. Jiang, IEEE Trans. Ultrason. Ferroelectr. Freq. Control **59**, 2548 (2012).
[21]Z. J. Chen, X. T. Li, J. G. Chen, and S. X. Dong, IEEE Trans. Ultrason. Ferroelectr. Freq. Control **60**, 115 (2013).
[22]Y. X. Liu, J. K. Liu, and W. S. Chen, IEEE Trans. Ultrason. Ferroelectr. Freq. Control **58**, 2397 (2011).